Originally distributed at the International Conference on Soldering and Reliability
Toronto, Ontario, Canada; May 20-22, 2009

PROBABILISTIC ASSESSMENT OF COMPONENT LEAD-TO-LEAD TIN WHISKER BRIDGING

S. McCormack and S. Meschter
BAE Systems
Johnson City, NY, USA
stephen.a.mccormack@baesystems.com

ABSTRACT
As a result of a global movement away from using lead (Pb) in electronic assemblies, component manufacturers are increasingly applying Tin-rich finishes to the leads of their devices. Unfortunately, this can create a risk of Tin whisker formation that can result in electrical failures if the gap between two adjacent component leads is bridged by a whisker. If bridging occurs, the effects can range from no effect to parametric system deviations to catastrophic circuit failure. Tin whisker risk management typically involves an evaluation of Tin plating attributes, base material of the component leads, underplating, lead-gap spacing, conformal coating, system use environment, and system reliability requirements. As an integral part of this management, a computational framework capable of quantifying the risk associated with Tin whisker-bridging failures is needed so that appropriate design, maintenance, and warranty decisions can be made. In the present work, a probabilistic model based on measured whisker observations is constructed. The model uses Monte Carlo simulation methods and quantifies the risk of Tin whiskers bridging the gap between two adjacent component leads. A dual-tail constraint strategy for constructing the whisker length probability density functions was established and applied to long and short-term bright Tin whisker length measurements. A bridging risk map also was developed to illustrate the relationship between lead-gap spacing, years of service life, and bridging risk. It was found that forming non-dimensional lead-gap spacing parameters provided useful insight into the risk posed by Tin whiskers.

Key Words: Tin Whisker Bridging Risk Monte Carlo

Nomenclature

General Model Parameters

N_{LS} = Number of lead side evaluation trials
N_{MC} = Number of whiskers simulated in the Monte Carlo analysis

Lead Geometry

L = Lead length
T = Lead thickness
G = Gap spacing between adjacent leads
G^* = Dimensionless gap spacing ($G/\rho_{0.998}$)
L^* = Dimensionless lead length = L/G
T^* = Dimensionless lead thickness = T/G
$P1$-$P8$ = Points used to define the (x, y, z) locations of the source and target areas of the lead sides.

Whisker Length Parameters

ρ = Tin whisker length
PDF_ρ = probability density function for whisker length
m = lognormal distribution shape parameter.
s = lognormal distribution location parameter
ρ_α = is the α *-fractile* value in a whisker length distribution. This is defined to be the length that is greater than or equal to an α fraction of all possible whisker length values[1]. Whisker lengths range from zero to infinity and α ranges from 0 to unity. (e.g. a distribution with $\rho_{0.998}$ = 525 microns indicates that 99.8 percent of all the whiskers will have a length less than or equal to 525 microns with 0.2% of them being greater than 525 microns).
α_l = left tail or lower fraction corresponding to the short whisker population.
α_u = right tail or upper fraction corresponding to the long whisker population.
$\rho_{\alpha l}$ = left tail or lower whisker length fractile corresponding to α_l.
$\rho_{\alpha u}$ = right tail or upper whisker length fractile corresponding to α_u.

Other Whisker Parameters

φ = whisker azimuth growth angle
PDF_φ = probability density function for whisker azimuth growth angle
θ = whisker rotational growth angle
PDF_θ = probability density function for whisker rotational growth angle
x = whisker base X coordinate
PDF_x = probability density function for the whisker base X coordinate
y = whisker base Y coordinate
PDF_y = probability density function for the whisker base Y coordinate
$P9$ = the (X,Y,Z) location of the base of a whisker
$P10$ = the (X,Y,Z) location of the tip of a whisker
$P11$ = the (X,Y,Z) location of the intersection point of the whisker and the target plane
PDF_{WD} = probability density function for whisker density
FWD = Whisker density factor used to evaluate reductions in baseline whisker density.

Model Outputs

N_B = Number of bridging whiskers
R_1 = Whisker risk metric in units of bridges/mm^2 of lead side area
R_2 = Whisker risk metric in units of bridges/lead side.

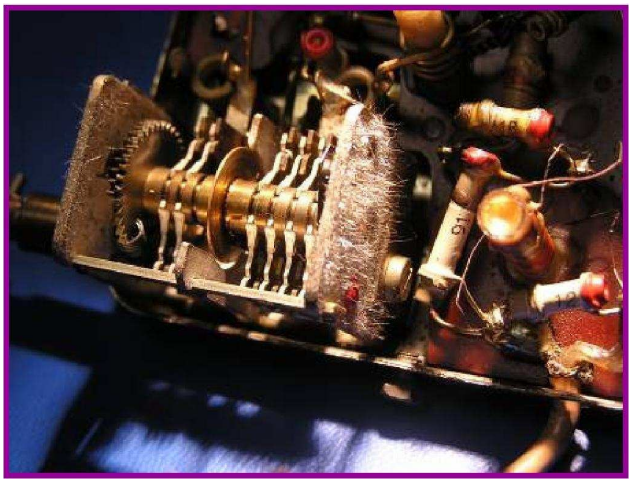

Fig. 1: Tin Whiskers on 1960s-Era Variable Air Capacitor [5]. Reproduced with permission from NASA

INTRODUCTION

Recent legislation on the reduction of hazardous substances (RoHS) from the European Union [2] and current environmentally friendly market trends [3] have resulted in the elimination of lead (Pb) from many electrical and electronic assemblies. Lead-free, Tin-rich finishes are increasingly being used in place of heritage Tin-lead finishes due to their low cost and metallurgical compatibility with the new Pb-free and heritage Sn-Pb solder systems. Unfortunately, as is shown in Fig. 1, Tin finishes not having at least 3% Pb are susceptible to spontaneous growths of filament-like structures commonly referred to as Tin whiskers [4][5]. These filaments are created by solid-state transport mechanisms that do not require vacuum or electrical bias. It has been theorized that whiskers are a form of recrystallization or crystal growth driven by stress or excess energy [6]. Sources of stress arise from intrinsic and extrinsic sources. Intrinsic sources include grain boundaries, dislocations, plating contamination (such as hydrogen, carbon, oxygen, etc.), and porosity. Extrinsic sources include coefficient of thermal expansion mismatch, reactions between the base layer and the Sn film, exposure to temperature, time, and humidity, electric current, mechanical bending, and Sn oxidation [6][7].

These whiskers are problematic because they are electrically conductive and can result in electrical leakage or shorting between conductors [5], metal vapor arcing or plasma at low pressure [8], and damage due to debris [9]. Recently, industry specifications have been established to address Tin whisker risk in electronic equipment [10][11]. The problem of Tin whiskers is not new and investigations into the phenomena date back to the 1950s [12]. Even though aerospace and military applications are exempt from the European Union legislation, they are dependent on commercial, off-the-shelf (COTS) electronic piece parts. The Pb-free transition continues to be disruptive to high-performance applications needing to assure reliable, repairable, certifiable, airworthy, supportable, affordable, and safe systems over a service life many times longer than is typical of COTS applications [13].

Given the high incidence of Tin-finished COTS piece parts, an assessment of the Tin whisker reliability risk must now be incorporated into the piece part selection and assembly design process if customer and end-user needs are to be satisfied.

The modeling described herein uses a geometric and proximity-based Monte Carlo simulation approach that solves the three-dimensional geometry problem and determines the risk of bridging between adjacent leads of a typical microcircuit as shown in Fig. 2. The evaluation cases were guided by scenarios of interest to the authors and used typical lead thicknesses, lead lengths, and lead-gap spacings. Monte Carlo analysis is an effective technique that has been used to assess the Tin whisker risk from a probabilistic perspective [14] [15] [16]. The relative risk levels of various configurations can be quantified and subsequently used to evaluate the need for additional whisker piece part or assembly-level mitigation strategies in an electronic system. [17]. The Monte Carlo simulation method also can be useful when considering the application of a higher-level system-risk calculator like the one developed by Pinsky [18]. Because the longest whiskers are the ones that likely will cause first failures, one of the biggest modeling difficulties lies with the probability distributions needed for the Monte Carlo analysis, particularly the length distribution as it varies over time. While it is clear that there are many factors that contribute to the growth of Tin whiskers [6] [19] [20] [21] (and fully characterized long-term Tin whisker data is lacking), these deficiencies eventually will be overcome via continuing research studies. In the present work, the probability distributions governing whisker length were determined from meshing short-term (six-month to 18-month) whisker length measurements of Fang [22] and the longer-term (three- to 15 ½-year) "maximum" whisker length data from experiments performed by Dunn [23] [24].

MODEL STRUCTURE

The configuration of microcircuits and other electronic devices can be relatively complex. As shown in Fig. 2, the spacing between the leads varies and the portion of the lead adjacent to the molding compound can have a dam bar shear area that has the narrowest lead-gap spacing.

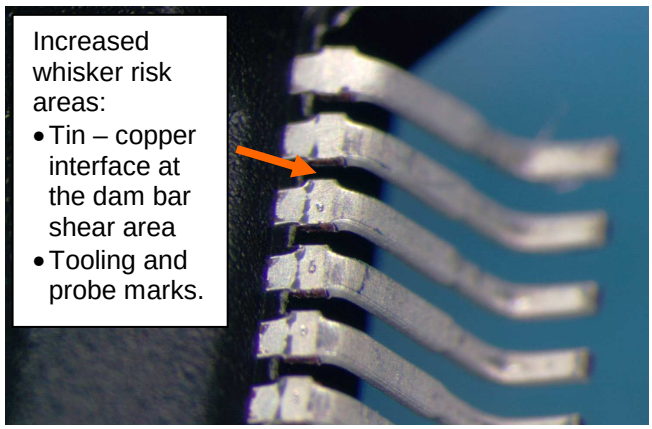

Fig. 2: Photomicrograph of fine-pitch microcircuit leads

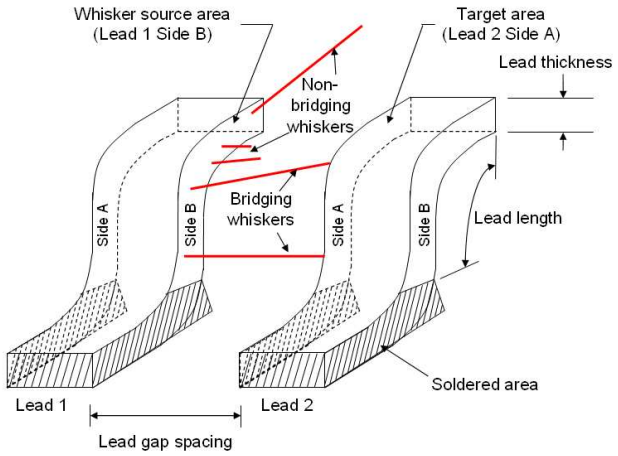

Fig. 3: Schematic diagram of leads with bridging and non-bridging whiskers traversing the gap between the leads showing Lead 1 Side B and Lead 2 Side A participating in the bridging risk

The dam bar shear area is often copper, and although not a source for whiskers, the boundary between the copper and the Tin is a dissimilar metal region susceptible to corrosion-induced whiskering [6] in high-humidity environments. In the present analysis, the bridging risk between one pair of adjacent leads (shown schematically in Fig. 3) was evaluated. Of the four lead sides shown, two are allowed to contribute to the bridging risk. Lead 1 side B is taken to be the source area, where the whisker base is located, and Lead 2 side A is the target area on the adjacent lead, where the short-circuit risk exists. In general, these leads may or may not be attached to the same component. The model allows whiskers to originate from the source area (Lead 1 side B) located on the source lead. Both the source and target areas are defined by their effective lead lengths and their lead thicknesses. This approach will allow the bridging risk associated with any number of leads and lead sides to be determined.

Major Modeling Assumptions

In any simulation, several practical assumptions need to be made in order to limit the scope and size of the modeling effort. The dominant conservative and anti-conservative assumptions are listed below.

Conservative (or benefit-ignoring) assumptions were made as follows:

1. Whiskers are mechanically robust, linear structures that are not kinked, twisted or exhibit curvature in three dimensional space.
2. No breakage of the whisker takes place prior to the whisker reaching its full and final length.
3. No credit is taken for advertent "whisker refreshing" provided by a periodic cleaning or removal of whiskers on the lead surfaces. Inadvertent refreshing caused by blowing fans, normal handling, etc., also is not taken into account.
4. Although it is possible for a bridged whisker to open as a result of its current carrying capacity being exceeded, no such fusing credit is taken.
5. No minimum threshold voltage is used for electrical conduction (current flow) to take place.

In addition to conservative assumptions, it was necessary to make the following anti-conservative (or risk-ignoring) assumptions:

6. No whisker-to-whisker interaction shorting takes place due to whiskers growing from other surfaces toward the source surface being analyzed.
7. Whiskers that have detached from the source lead and pose a "loose-whisker" conductive debris-shorting risk are not taken into account.
8. Details associated with lead forming and specific lead micro-geometry were not included, since a simplified finite parallel plate geometry was used.
9. Whiskers originating from and making contact with the front and back surfaces of the leads were not considered.
10. Whisker deflection due to external loads such as acceleration, airflow, or electric fields were not considered.

Two other assumptions and model limitations that don't fit into either of the above categories needed to be made. These are:

11. No detailed chemistry, materials science, or growth physics are explicitly included, since the growth theory has not been fully worked out. These details are implicitly embodied in the experimental whisker results used to define the PDFs.
12. No direct environmental effects such as voltage, humidity, or thermal cycling were taken into account.

Analytic Geometry

The simplified analytic geometry that was solved for each whisker simulated is summarized in Fig. 4. Here the source area is defined by four corner points, *P1* through *P4*, which are located in three-dimensional space. For convenience, the origin of the Cartesian Coordinate Systems is located at *P1*. Likewise, the target area is defined by *P5* through *P8* and is translated along the *Z* axis a distance equivalent to the lead-gap spacing. The model is flexible in that the source and target areas need not be the same size or parallel to each other, but a parallel plane arrangement is used to simplify the present evaluations. The base of the whisker is defined as *P9* and is restricted to lie somewhere within the source area. One length and two independent angles are needed to define a straight whisker in three-dimensional space. The growth angle φ is defined as an angle from a perpendicular from the source area; the rotational angle is defined by revolving an angle about the base of the whisker and is defined as θ. Fig. 4 shows a whisker having length, ρ, with these angles.

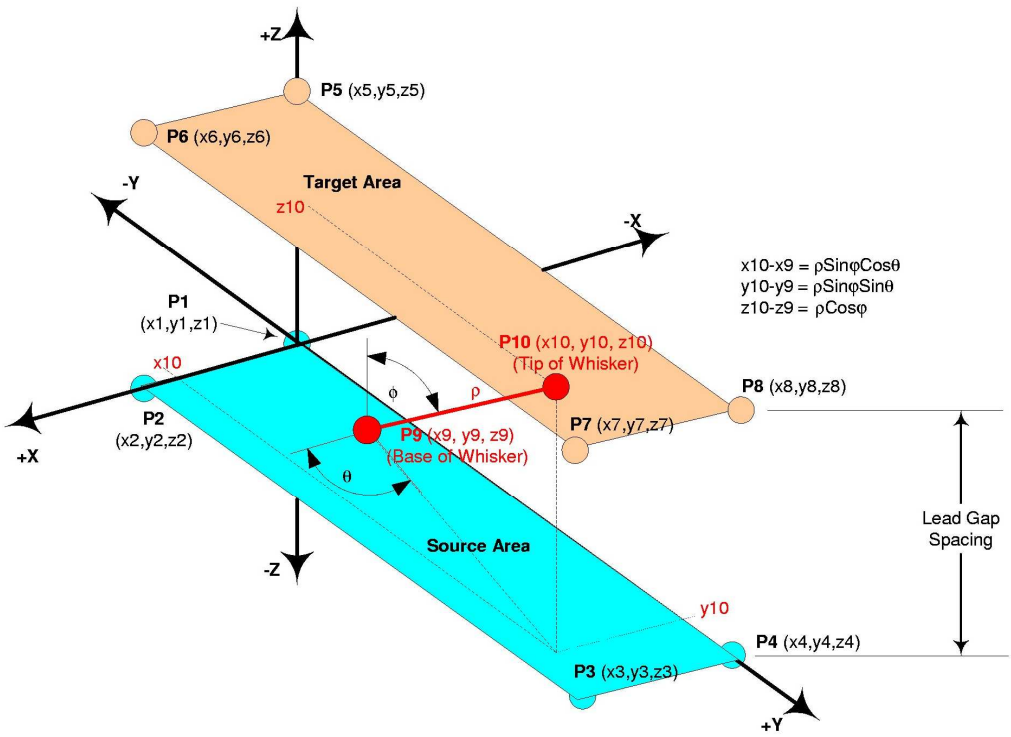

Fig. 4: Model geometry for the rectangular simplified model where lead length, $L = y_4-y_1$, lead thickness, $T = x_2-x_1$, and lead-gap spacing, $G = z_5-z_1$.

Once the base coordinates, whisker length ρ, and angles, θ and φ, are sampled from the respective probability density functions, the location of the tip of the whisker *P10* can be determined by solving eqs. 1, 2 and 3.

$$x10 - x9 = \rho Sin\varphi Cos\theta \quad (1)$$
$$y10 - y9 = \rho Sin\varphi Sin\theta \quad (2)$$
$$z10 - z9 = \rho Cos\varphi \quad (3)$$

Likewise, the coordinates of the intersection point *(x11, y11)* of the whisker and the plane containing the target area can be computed from eqs. 4 and 5.

$$x11 - x9 = \rho_2 Sin\varphi Cos\theta \quad (4)$$
$$y11 - y9 = \rho_2 Sin\varphi Sin\theta \quad (5)$$

Where ρ_2 is defined as the length along the whisker from the base to the target-area plane and is described by eq. 6.

$$\rho_2 = \frac{\text{gap spacing - z9}}{\cos(\varphi)} \quad (6)$$

Bridging Failure Definition

For a whisker to cause a bridging failure, two fundamental requirements must be met. First, the length of the whisker must equal or exceed the spacing between the leads. And second, the (*x*, *y*) location of the whisker base must combine with the growth angles in an unfavorable way so that the whisker will intersect the target area. Fig. 3 depicts examples of bridging whiskers and non-bridging whiskers. From an analytical perspective, this also includes the case where the whisker has penetrated the target surface. Determining whether a given whisker has bridged was accomplished by applying two geometrical tests to each whisker simulated. Test #1 determines if the z-coordinate of the tip of the whisker is less than the lead-gap spacing. If this test returns a "true," then it is not possible for bridging to occur and no further testing is required for that whisker. If Test #1 returns a "false," then it is possible for bridging to occur and a second test is needed. Test #2 determines the *x*- and *y*-coordinates of the point on the whisker that has a z-value equal to the lead-gap spacing. If these (*x*, *y*) coordinates lie within the area bounded by the target area (*P5 – P8*), then the whisker is counted as a bridge. Otherwise, the whisker is counted as a non-bridge.

The authors have chosen two bridging-risk metrics to convey the risk associated with a given scenario. The first metric is the number of whisker bridges per square millimeter of participating lead side area, which can be used to obtain a sense of how the number of bridges between a lead pair scales with area. The second metric is reported as bridges per lead side for a given lead geometry. These are referred to herein as R_1 and R_2. After the many thousands of whiskers for a given Monte Carlo simulation have been simulated and assigned either a "bridged" or "not-bridged" status. The metric, R_1 is defined by:

$$R_1 = \frac{\text{Total Number of Bridges}}{A_s * N_{LS}} [\text{bridges/mm}^2] \quad (7)$$

where A_s is the source area of a single lead side [mm^2], N_{LS} the number of Monte Carlo lead side trials, which is equal to the number of lead sides analyzed. The second metric R_2 is defined as:

$$R_2 = \frac{\text{Total Number of Bridges}}{N_{LS}} \text{[bridges/lead side]} \quad (8)$$

Simulation Strategy

The inputs, intermediate outputs, and final outputs of the Monte Carlo simulation are summarized in Fig. 5. The general purpose mathematics and programming package *Mathematica* © [25] was used to program and execute the simulation logic shown in Fig. 6 so that the bridging results for various scenarios could be determined. An evaluation begins with establishing the desired number of whiskers to simulate. Since the area of an individual lead side surface is not likely to contain a statistically significant number of whiskers, it was decided that generating approximately half-million whiskers per analysis case provided a reasonable compromise between execution time and statistical robustness. Next, the basic constants needed to define the lead-gap spacing and the source and target area corner points were specified. The required probability density functions are specified next. In this analysis, evaluations are repeated on multiple lead sides until a minimum of half-million whiskers have been simulated in total. Each lead side evaluation is called a "trial" and the number of lead side trials, N_{LS}, was increased until enough whiskers have been simulated to achieve the goal of half-million whiskers. Typically, N_{LS} was between 10,000 and 30,000 for the lead geometries under consideration. The number of trials is then computed, which represents the number of individual lead pairs that are to be simulated. A list of whisker-density values is then generated with one density value assigned to a each source area. This allows a discrete number of whiskers to be populated across the source area. The total number of whiskers is then determined from the summation of those on the individual source areas. Next, random values for φ, θ, *x9*, *y9*, and ρ are sampled from the probability density functions. The whisker tip coordinates *x10*, *y10* and *z10* are then calculated and the coordinates of the intersection point of the whisker and the target plane area are computed.

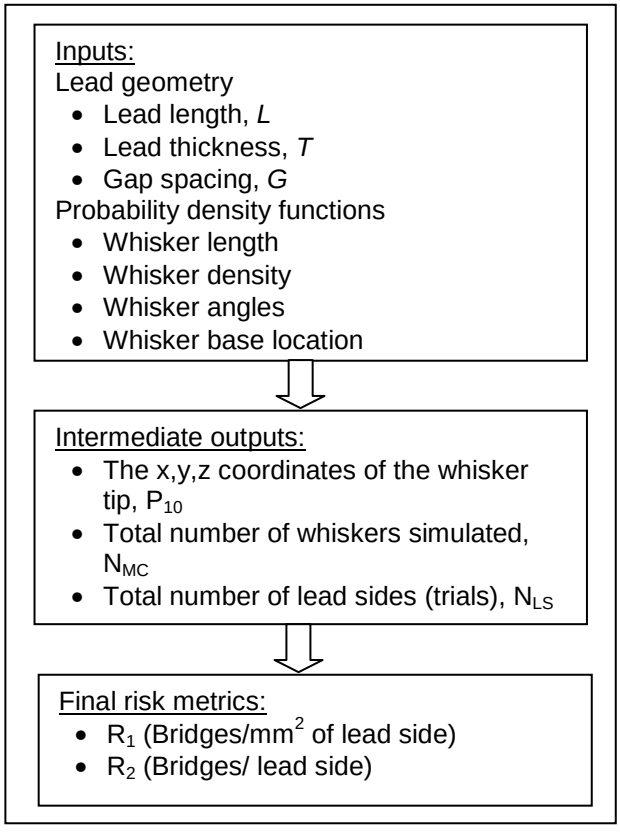

Fig. 5: Model inputs and outputs

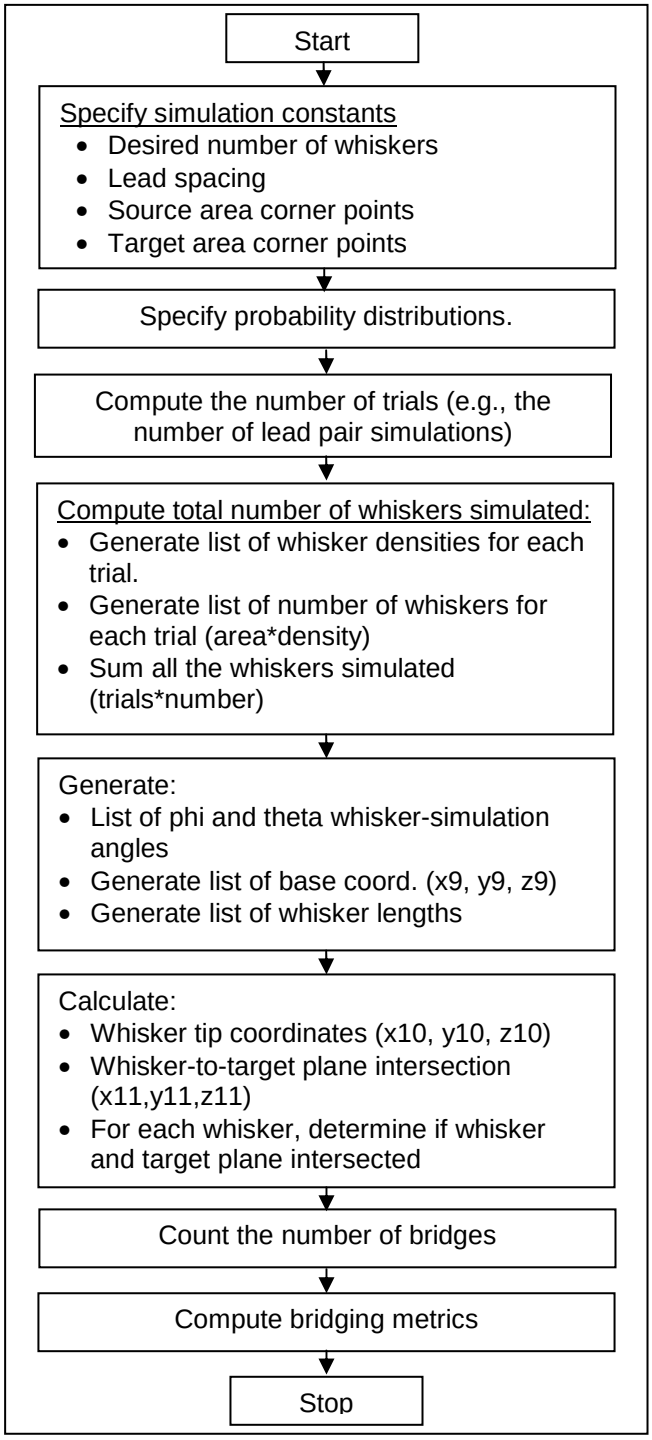

Fig. 6: Simulation Logic

For each whisker simulated, a determination is made as to whether it came into contact (or penetrated) the target area, thus allowing the total number of bridges to be determined. Finally, the bridging density is determined from the number of bridges, the number of trials, and the source area.

Probability Distributions

The six probability density functions used in the Monte Carlo simulations were for the following parameters: (1) whisker base "*x*" location, (2) whisker base "*y*" location, (3) whisker rotation angle, θ, (4) whisker azimuth angle, φ, (5) whisker area density, and (6) whisker length, ρ. The distribution types are given in Table 1. The definition of these probability-density functions, along with a detailed description of the development of the area-density, angle-distribution, and whisker-length functions are discussed next.

Whisker Base Position Distributions

The whisker base positions were distributed uniformly in the *x* and *y* direction on the source area being analyzed. Typical distributions are given in Fig. 7 and Fig. 8.

Whisker Angular Growth Direction Distributions

The stepwise continuous distribution for the whisker azimuth angle, φ, from Table 2, as shown in Fig. 10, was used in the present study. The whisker rotational angle, θ, was taken to be a uniform distribution that varies from zero to 360 degrees, as shown in Fig. 9.

Whisker Density Distribution

A normal distribution for the whisker density (whiskers per mm^2) based on the measurements by Fang [22] for bright-tin plating was used as a baseline. However, various whisker-density PDFs were selected to explore the effect on bridging risk. Since the authors are unaware of supporting test data to the contrary, the mean was allowed to scale with the standard deviation.

Table 1: Tin Whisker Probability Distributions used in the Monte Carlo Simulation

PDF	Distribution Type	Parameters
PDF_x for *x* direction of whisker location on source area	Uniform	Fig. 7
PDF_y for *y* direction of whisker location on source area	Uniform	Fig. 8
PDF_θ for Whisker Rotation Angle, θ	Uniform	Fig. 9
PDF_φ for Whisker Azimuth Angle, φ	Stepwise continuous	Table 2 and Fig. 10
PDF_{WD} for Whisker Density	Normal	Table 3 and Fig. 11
PDF_{LW} for Whisker Length, ρ	Lognormal	Table 5

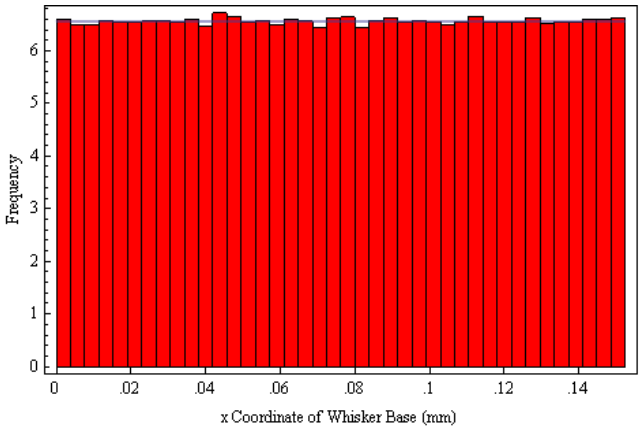

Fig. 7: Histogram plot superimposed on the PDF showing the typical *x* coordinates of whisker base point. Type: uniform, minimum = 0, maximum = 0.1524 mm shown. This PDF varies as lead geometry type changes

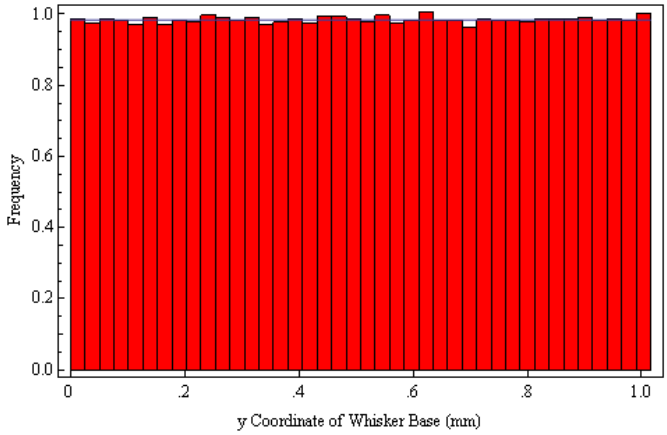

Fig. 8: Histogram plot superimposed on the PDF showing the typical *y* coordinates of whisker base point. Type: uniform, minimum = 0, maximum = 1.016 mm shown. This PDF varies as lead geometry type changes

Table 2: Whisker azimuth angle, φ, distribution used in the Monte Carlo evaluation

Angle Range (degrees)	Percentage
0~10	15.4
10~20	20.5
20~30	18.1
30~40	13
40~50	11.4
50~60	6.7
60~70	7.9
70~80	4.3
80~90	2.7

(Note the angles given by Fang [14] were subtracted from 90 degrees so that each matches the definition of whisker angle, φ, shown in Fig. 4 and Fig. 10).

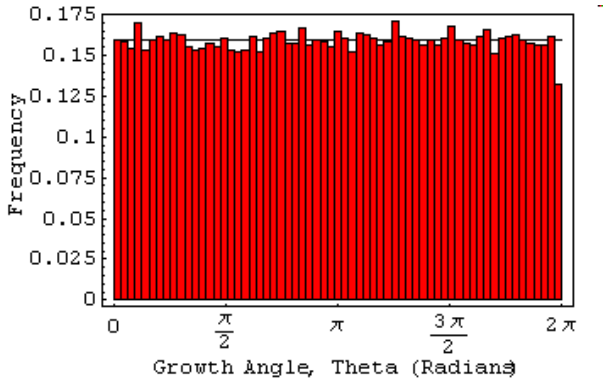

Fig. 9: Whisker growth rotation angle, θ, distribution. Type: uniform, minimum = 0 radians, maximum = 2π radians

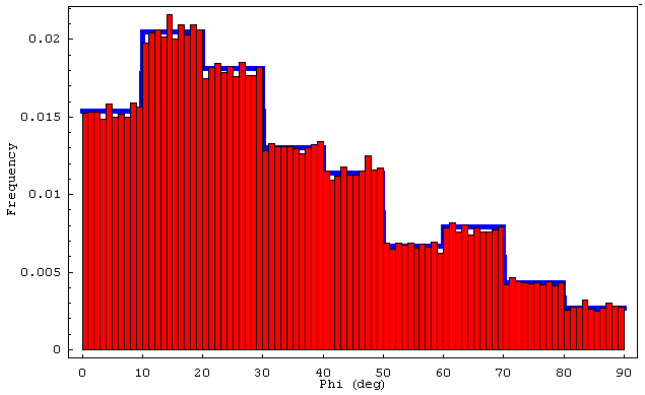

Fig. 10: Whisker growth azimuth angle, φ, distribution. Type = Custom, minimum = 0 degrees, maximum = 90 degrees

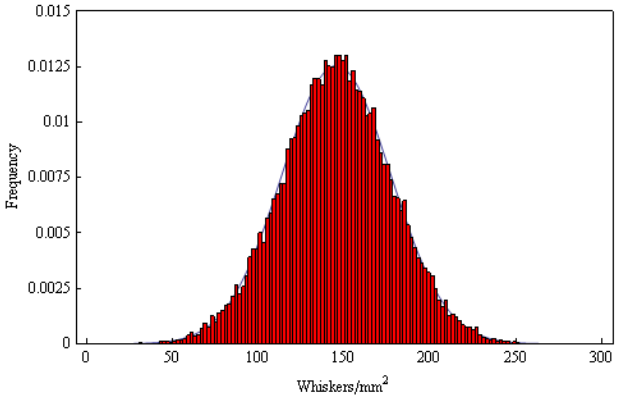

Fig. 11: Whisker Density Distribution after Fang [22]. Type = Normal, Mean = 145.2 whiskers/mm^2 (93683 whiskers/in^2), Standard Deviation = 31.8 whiskers/mm^2 (20517 whiskers/in^2)

This was accomplished by multiplying the mean and the standard deviation by the parameter F_{WD}. Fig. 11 illustrates the whisker density distribution for F_{WD} equal to one, which corresponds to Fang's bright-tin measured values (mean = 145.2 and standard deviation = 31 whiskers per mm^2) [22]. Here, F_{WD} is varied from 1 to 0.1, as shown in Table 3, to evaluate lower whisker densities that may be encountered with different Tin platings and environmental exposure. For example, annealed matte Tin over Copper exposed to

Table 3: Whisker density Probability Density Functions Evaluated

PDF_{WD} Distribution Number	Mean (whiskers per mm^2)	Std Dev (whiskers per mm^2)	Fraction of density distribution number 1
1	145.2 [22]	31.8	1
2	96.8	21.2	2/3
3	48.4	10.6	1/3
4	14.5	3.2	1/10

50°C/50%RH for 1.5 years and room condition 25 °C for 2 years was reported to have a whisker density of 48 whiskers per mm^2 [26]. In addition, Fukuda, et. al., [27] recently reported the whisker density for matte Tin plating over copper after 16 months at room temperature to have a mean whisker density value of only four whiskers per mm^2.

Whisker Length

Highly controlled whisker growth experiments tend to be relatively short in duration when compared to the needs of many aerospace and military requirements [15] [22] [26] [27]. In addition, many of these controlled experiments lack sufficient diversity in sample sizes, substrate materials, plating types, and real-world environmental conditions. For instance, Fang, et. al., [22] applied bright-tin plating over brass to obtain Tin whisker growth data on samples examined over 18 months. Moreover, with the exception of one experiment that was started in the 80s and continues to the present day, there is no long-term Tin whisker data that the authors are aware of. In the aforementioned assessment that began in the 80s, 15-½ year whisker growth data was reported for bright-tin over copper-plated brass C-Ring specimens subjected to various amounts of mechanical stress and maintained in a desiccated environment [23] [24]. Unfortunately, this data set does not include information on whisker length distribution, area density, or growth angle. In addition, the plating used by Dunn was a bright-tin plating and is not regarded as a modern, "low-whisker-propensity-" plating chemistry. However, it is interesting to note that when the initial Dunn measurements were terminated in 1987, the whisker growth was observed to have essentially stopped [23]. However, upon re-examination of these same specimens, which were maintained in a desiccated environment until 2006, significant additional growth was observed on many of the specimens, particularly on platings that were deposited over a copper barrier [24]. The long whiskers observed in the Dunn desiccated experiment may be somewhat representative of "real whisker growth". While many devices don't use bright-tin plating, many of the "real-world" applications do not have the benefit of being in a clean desiccated environment. In real-world applications, a matte-tin plating could be exposed to humid and corrosive conditions, thus suggesting that the Dunn measurements of bright Tin may not be as overly conservative as one might initially think.

Table 4: Maximum Whisker Length Data Source: Ref. [24], Specimen 11

Time Duration (days)	C-Ring Location			
	A	B	C	Avg. of the maximums
3	50	50	50	50
27	200	100	50	116.67
57	500	140	60	233.33
142	500	200	100	266.67
181	500	600	100	400
634	500	600	100	400
1269	500	600	100	400
2920				525(1)
5657	700	1000	500	733.33

Note 1: Note the 2920-day (eight-year) average value was obtained by linearly interpolating between 1269 and 5657 days. Recently, investigators have found that long whisker growth was augmented by corrosion induced by the presence of liquid water on whisker-resistant Tin platings [6] [28].

Strategy for constructing the whisker length PDF

The authors are unaware of statistically significant data sets that describe whisker lengths over time periods exceeding a decade that are suitable for direct probabilistic risk analysis. Many of the whisker-length studies report "maximum" whisker lengths after specific time periods under a specific set of environmental conditions. Therefore, a strategy was needed that could use long-term and short-term published whisker-length observations. Similar to the approach used by Fang, et. al., [22] and Fukuda, et. al., [27], the present approach exploits the lognormal probability distribution to describe whisker length. This distribution embodies the general observation that Tin whisker populations tend to have many shorter whiskers and fewer longer ones. The probability density function describing the lognormal distribution is given by:

$$PDF_{LW} = \frac{e^{-\frac{(\ln[\rho]-m)^2}{2s^2}}}{s\rho\sqrt{2\pi}} \quad (9)$$

where ρ is whisker length, m is the location parameter, and s is the shape parameter. Eq. (9) for a specific pair of m and s parameters was plotted in Fig. 12A. Note that the total area under this curve (as also is required by all other PDFs) is equal to unity.

The lognormal probability-density function of Fig. 12 represents the statistical frequency of the physical length of a Tin whisker. Corresponding to any given length value, ρ, on the abscissa is an associated fraction, α, which is the fraction of all length values that are less than or equal to the given ρ value and ranges from zero to unity. The whisker length, ρ_α, is therefore the whisker length that is greater than or equal to an α fraction of all values. Since the total area under the PDF is equal to unity, α can be mathematically determined by integrating the PDF from zero to the ρ_α.

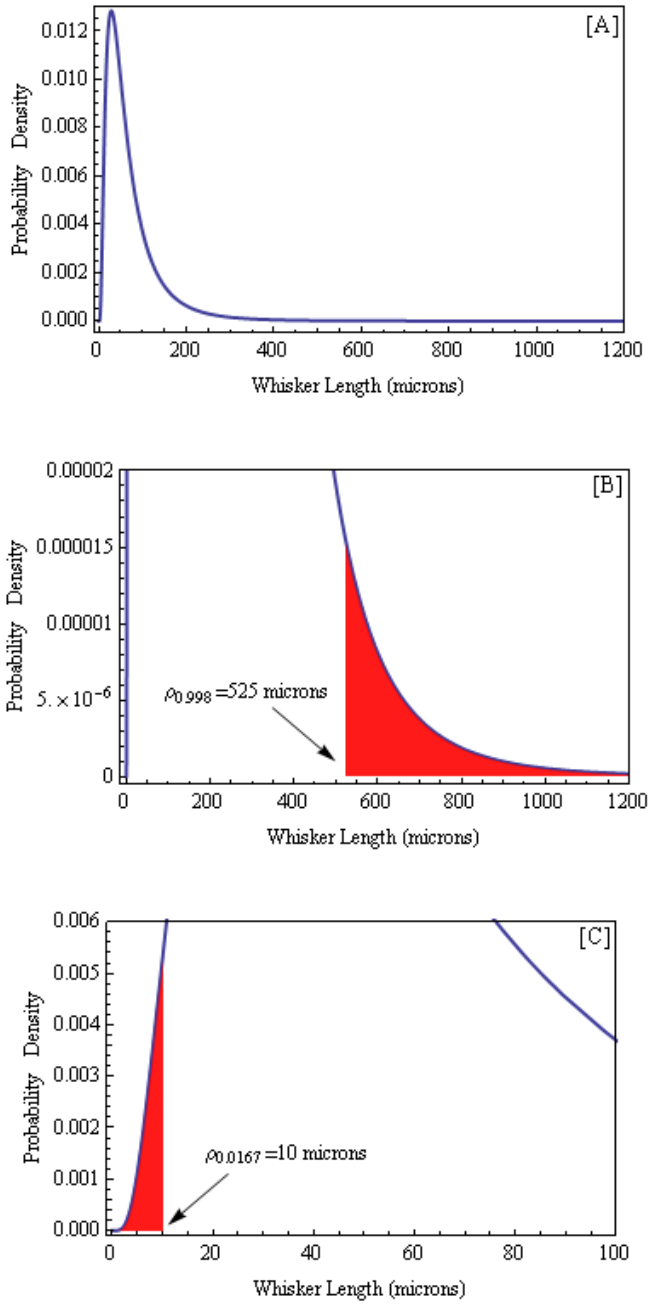

Fig. 12: Sample lognormal PDF for whisker length. (A) the PDF shown up to 1200 microns, (B) the right tail upper whisker length fractile, $\rho_{0.998}$ = 525 microns, with the shaded area = 0.2% and (C) the left tail lower whisker fractile, $\rho_{0.0167}$ = 10 microns, with the shaded area = 1.67%

Specific location and shape parameters (m, s) for a given evaluation case were computed by imposing two constraints on the distribution. The first constraint established the right-tail behavior by requiring that the specified upper whisker length fractile, $\rho_{\alpha u}$, corresponds to the maximum experimentally measured whisker length as shown in Fig. 12B.

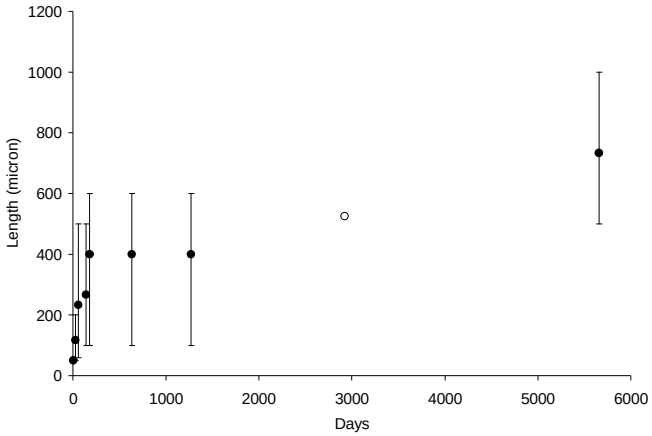

Fig. 13: Average maximum whisker length versus time for Dunn specimen 11 (normal electroplated bright Tin over brass with a copper underplating) [23][24]. The error bars indicate the maximum whisker length variation reported from the three C-Ring test specimen locations used to obtain the average value. The open symbol was computed using a linear interpolation between 1269 and 5657 days

The second constraint established left-tail behavior in a similar manner, except that the specified lower whisker length fractile, $\rho_{\alpha l}$, was chosen to be 10 microns (the minimum-measured whisker length) as shown in Fig. 12C. By simultaneously imposing these dual constraints, the desired behavior of both tails of the distribution is assured. The baseline fractile values used herein for the left and right tails were $\rho_{0.0167}$ = 10 microns and $\rho_{0.998}$ = 525 microns. The left-tail α_l value of 0.0167 corresponds to the fraction of whiskers that are 10 microns in length or shorter in the Fang lognormal distribution for the 18-month data set [22].

The α_u value of 0.998 was selected because it corresponds to the fraction of whiskers that were equal to or longer than 80 microns (the longest observed in the 18-month data) in the Fang lognormal distribution data [22].

For the present analysis, Dunn specimen 11 [24] was used as the basis for the maximum whisker length as a function of time. Specimen 11 was "normal" bright-tin plating over copper-plated brass and did not represent the shortest or the longest growth case; rather, among the bright-tin platings, it represented a "middle-of-the-road" case. In addition, it was one of the specimens that exhibited a resumption in growth after the initial 3.5-year interval [23]. In the present work, the $\rho_{0.998}$ was taken to be the average of the maximum whisker lengths measured from the three stress regions of the C-Ring specimen. (Note: Dunn indicated that whisker growth did not correlate to stress location on the C-Ring specimens). These "average-maximum" values are given in Table 4 and plotted in Fig. 13.

The aforementioned strategy for constructing whisker length PDFs was repeated several times for combinations of tail percentages and maximum fractile lengths of interest so that the effects of the resulting PDFs upon bridging risk could be studied.

The majority of the upper-fractile whisker lengths were selected such that they corresponded to the experimental observations made by Dunn [24]. Since these observations were made at specific time intervals, these constructed PDFs can be associated with a unique duration. Table 5 tabulates *m* and *s* for these combinations.

Table 5: Lognormal Tin Whisker Length Distributions for various ρ_α tail parameters

Dist. No.	α_l	α_u	$\rho_{\alpha l}$ (microns)	$\rho_{\alpha u}$ (microns)	Time (years) (1)	m	s
1	0.016963	0.988	10	400	0.5 and 3.5	3.86765	0.737907
2	0.016963	0.998	10	525	8	3.9833	0.792435
3	0.016963	0.998	10	733	15.5	4.12481	0.859156
4	0.016963	0.998	10	200	NA	3.57357	0.599253
5	0.016963	0.998	10	500	15.5	3.96232	0.782544
6	0.016963	0.998	10	1000	15.5 (2)	4.2564	0.921198
7	0.016963	0.998	10	3000	NA	4.7225	1.14096
8	0.016963	0.998	10	4600	15.5 (3)	4.90385	1.22646
9	0.016963	0.9998	10	525	8	3.78653	0.699663
10	0.016963	0.98	10	525	8	4.31487	0.948766
11	$1x10^{-11}$	0.998	10	525	8	5.07395	0.413266
12	0.001696	0.998	10	525	8	4.30057	0.681971
13	0.17	0.998	10	525	8	3.28874	1.03353

Notes:

1. The times given correspond to average-maximum whisker length observations reported by Dunn [24] for specimen 11 as shown in Fig. 13, unless otherwise specified.
2. The $\rho_{0.998}$ of 1,000 microns corresponds to the maximum whisker length observed for specimen 11 after 15.5 years, rather than the average of the maximums.
3. The $\rho_{0.998}$ of 4600 microns corresponds to the maximum whisker length observed for all the specimens tested by Dunn [24] after 15.5 years.

Table 6: Summary of Evaluations

Parameter examined	Varied parameters (lengths in microns)	Fixed-distribution parameters (1) (lengths in microns)	Fixed-geometry parameters (lengths in microns)	Results
Typical geometry	None	F_{WD} = 1 $\rho_{0.01696}$ = 10 $\rho_{0.998}$ = 525	T = 152.4 L = 1016 G = 457.2	R_1 = 0.1175 bridges/mm^2 R_2 = 0.0182 bridges/lead side
F_{WD}	0.1 ≤ F_{WD} ≤ 1	$\rho_{0.01696}$ = 10 $\rho_{0.998}$ = 525		Fig. 14
α_u	0.98 ≤ α_u ≤ 0.9998	F_{WD} = 1 $\rho_{0.01696}$ = 10 $\rho_{\alpha u}$ = 525		Fig. 15
α_l	1x10^{-11} ≤ α_l ≤ 0.17	F_{WD} = 1 $\rho_{\alpha l}$ = 10 $\rho_{0.998}$ = 525		Fig. 16
$\rho_{0.998}$	0.099 ≤ G* ≤ 2.286 4600 ≥ $\rho_{0.998}$ ≥ 200	F_{WD} = 1 $\rho_{0.01696}$ = 10		Fig. 17
Lead gap spacing	0.435 ≤ G^* ≤ 1.45 228.6 ≤ G ≤ 762	F_{WD} = 1 $\rho_{0.01696}$ = 10 $\rho_{0.998}$ = 525	T = 152.4 L = 1016	
Lead thickness	0.0556 ≤ T^* ≤ 1 25.4 ≤ T ≤ 457.2		L = 1016 G = 457.2	Fig. 18
Lead length	0.0556 ≤ L^* ≤ 5.56 25.4 ≤ L ≤ 2540		T = 152.4 G = 457.2	Fig. 19

Dimensionless Parameters

There were several convenient ways of non-dimensionalizing the lead geometry. For the lead thickness, T, and the lead length, L, lead-gap spacing, G, was used for scaling to obtain

$$T^* = \frac{T}{G} \qquad (10)$$

$$L^* = \frac{L}{G} \qquad (11)$$

where T^* is the dimensionless lead thickness and L^* is the dimensionless lead length. For the lead-gap spacing, it was apparent that whiskers having length less than the gap spacing will not cause a bridging failure. Therefore, a dimensionless lead-gap spacing parameter, G^*, was defined as the ratio of the gap spacing, G and the $\rho_{0.998}$ whisker length given by:

$$G^* = \frac{G}{\rho_{0.998}} \qquad (12)$$

RESULTS AND DISCUSSION

Monte Carlo simulations were employed to assess whisker-bridging risk as changes were made to the whisker density and whisker length probability-density functions and the lead geometry. In the final section of the analysis, the whisker length and the gap spacing data was synthesized into a bridging risk map. The PDFs for whisker position, azimuth angle, and rotational angle were held constant for all evaluations. During various assessments, the lead thickness and length were held constant (T = 152 and L = 1016 microns), thus R_1 and R_2 are proportional to each other with R_2 being equal to R_1 multiplied by the area of the lead side (0.15484 mm^2). The risk parameters, R_1 (bridges/mm^2 of lead side) and R_2 (bridges/lead side) were used to compare the bridging risks for the various evaluation cases on a participating lead side basis. The analysis cases are summarized in Table 6 and Table 7. Note that these metrics are generically defined on an area and lead side basis, which allows the risks to be evaluated for any participating area and number of leads. For example, a 132-lead-quad flat-pack with four rows of n = *33* leads will have 64 (e.g., *2n-2*) participating lead sides in each row, resulting in a total of 256 participating lead sides for the device. If each lead side has an area of 0.15484 mm^2, the total participating area is 39.64 mm^2. In the case where the lead-gap spacing between leads is 457 microns and the expected whisker length is $\rho_{0.998}$ = 525 micron, then from Table 7 an R_1 of 0.121 bridges/mm^2 per lead side is obtained. The resulting total-device bridging risk is computed to be 4.8 bridges and, for high-reliability applications, additional mitigation would be needed in this situation.

Whisker Density

First, the whisker density distribution parameter was evaluated. The results shown in Fig. 14 reveal that the bridging risk is proportional to the whisker density. The whisker density used in the majority of the cases in the present analysis (mean = 145.2 whiskers/mm^2) represents Fang measurements for bright-tin plating [22] and is consistent with the plating used by Dunn [24]. However, most electrical components use matte-tin plating having a whisker density of approximately 50 whiskers per mm^2 [26], which is ~ 1/3 of the bright-tin plating whisker density. Reducing F_{WD} from one to 1/3 (e.g. from 145.2 to 48.4 whiskers/mm^2), resulted in reduction of bridges from 0.12 to 0.04 bridges per mm^2.

Table 7: Bridging risk map metrics for various lead-gap spacings, years and $\rho_{0.998}$ values (1)

Lead-gap spacing		Whisker characteristics		Dimensionless gap spacing	Bridging risk metrics	
G (microns)	G (inches)	Time (years)	$\rho_{0.998}$ (microns)	$G^* = G/\rho_{0.998}$	R_1 (bridges/mm^2)	R_2 (bridges/lead side)
228.6	0.009	0	0		0	0
		0.5, 3.5 (2)	400	0.5715	0.904	0.140
		8.0	525	0.4354	1.80	0.279
		15.5	733	0.3119	3.54	0.548
304.8	0.012	0	0		0	0
		0.5, 3.5 (2)	400	0.7620	0.281	0.0436
		8.0	525	0.5806	0.619	0.0959
		15.5	733	0.4158	1.470	0.227
381	0.015	0	0		0	0
		0.5, 3.5 (2)	400	0.9525	0.0942	0.0146
		8.0	525	0.7257	0.251	0.0389
		15.5	733	0.5198	0.689	0.107
457.2 (3)	0.018	0	0		0	0
		0.5, 3.5 (2)	400	1.1430	0.042	0.00657
		8.0	525	0.8709	0.121	0.0188
		15.5	733	0.6237	0.346	0.0535
533.4	0.021	0	0		0	0
		0.5, 3.5 (2)	400	1.0835	0.0159	0.00247
		8.0	525	0.8255	0.0566	0.00877
		15.5	733	0.5913	0.172	0.02657
762	0.030	0	0		0	0
		0.5, 3.5 (2)	400	1.9050	0.00284	0.00044
		8.0	525	1.4514	0.00910	0.00141
		15.5	733	1.0396	0.0404	0.00626

Notes

1. A constant lead thickness of 152 micron (0.006 inch) and a lead length of 1017 microns (0.040 inch) was used.
2. The 3.5-year (400-micron) results are used for the 0.5-year plateau value.
3. The data from Fig. 19 used for the 457.2-micron gap-spacing risk metrics.

Upper and Lower Whisker Length Fractions

In the long-whisker fraction evaluation, α_u was varied from 0.98 to 0.9998, while the whisker length was maintained to be $\rho_{\alpha u}$ = 525 microns. The result shown in Fig. 15 indicates a nearly proportional relationship between the bridging risk metrics and α_u. The results in Fig. 15 are rationalized in the following manner: The case where α_u is 0.998 and $\rho_{0.998}$ is 525 indicates that a 0.002 fraction of randomly chosen whiskers will be greater than or equal to 525 microns. Since a 525-micron whisker is capable of bridging a 457-micron gap, these whiskers will bridge the gap unless the angles and base-location random selections combine to prevent a bridge from occurring. If α_u is decreased to 0.98, then the fraction of whiskers greater than 525 microns is increased to 0.02 and there will then be an increase by a factor of 10 in the probable number of whiskers greater than 525 microns. As before, each of these additional whiskers is long enough to bridge the gap and therefore the number of bridges also is expected to increase by a factor of approximately 10, given that the PDF of the whisker azimuth angle, φ, is dominated by values close to zero (e.g. perpendicular to the source plane) and the lead thickness and length are being held constant. In contrast, Fig. 16 shows that the bridging risk was not significantly impacted when the fraction of short whiskers, α_l, was varied. These findings support the fact that the small population of long whiskers determines the whisker-bridging risk between adjacent electrical conductor leads. As will be seen in the next portion of the analysis, even though the relationship between α_u and bridging risk is proportional, the actual change in bridging risk is relatively small in comparison to the changes in bridging risk observed when $\rho_{0.998}$ was varied.

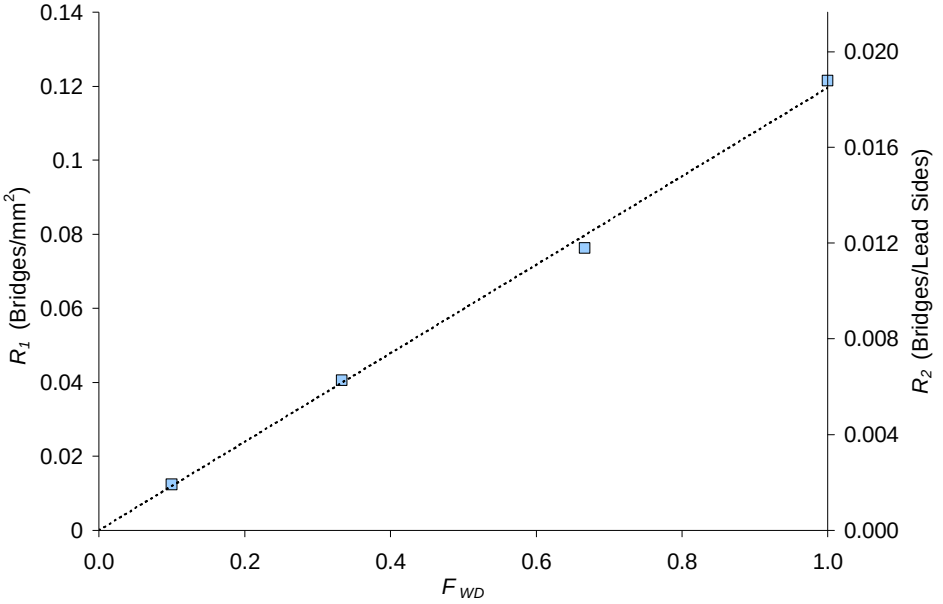

Fig. 14: Risk Metrics R_1 and R_2 versus whisker-density fraction, $F_{WD.}$ A whisker-density fraction equal to one corresponds to a mean-area density of 145.2 whiskers/mm^2 with a standard deviation of 31.8 whiskers/mm^2

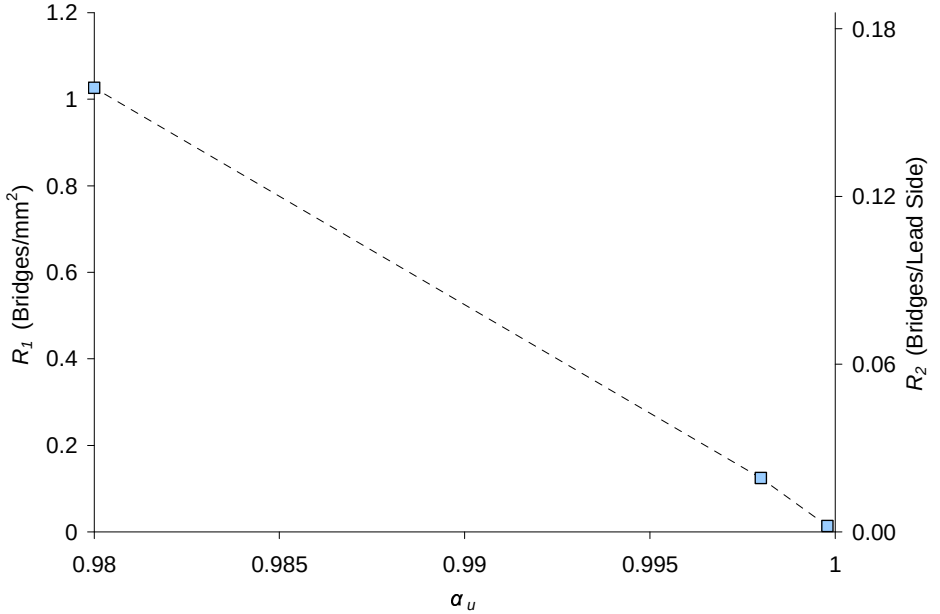

Fig. 15: Risk metrics R_1 and R_2 versus the upper whisker fraction, α_u

Dimensionless Lead-gap Spacing

It is expected that the "longest whiskers" will be the first to contribute to the whisker-bridging risk metrics. As the experimental measurements in Fig. 13 illustrate, even for the simple case of experimentally controlled Tin-plating samples maintained in a dry environment for more than a decade, the observed maximum whisker lengths exhibited large variations in magnitude and increased non-linearly with time. The relationship between the longest whisker and the gap spacing that must be traversed in order to create a bridging short is captured in the dimensionless gap spacing $G^* = G/\rho_{0.998}$. From the physical geometry of the leads, the gap spacing, G, generally varies from 229.8 microns (0.009 inches) to 762 microns (0.030 inches), while the whisker length can vary significantly depending upon process parameters, Tin plating parameters, environment, and duration.

Examining Fig. 17, the risk-metric values increased dramatically when $G^* < 1$. In the present study, a G^* of 2.286 with G = 457 microns and $\rho_{0.998}$ = 200 microns yielded the smallest magnitudes of R_1 and R_2 (0.000285 bridges/mm^2 and 4.4 x 10^{-5} bridges/lead side respectively). Given the likelihood that there would be 100 to 1,000 leads in a system, the bridging risk results imply that some applications would benefit from additional whisker mitigations such as hot-solder dipping [29] or conformal coating [10] [30] [31] [32] [33].

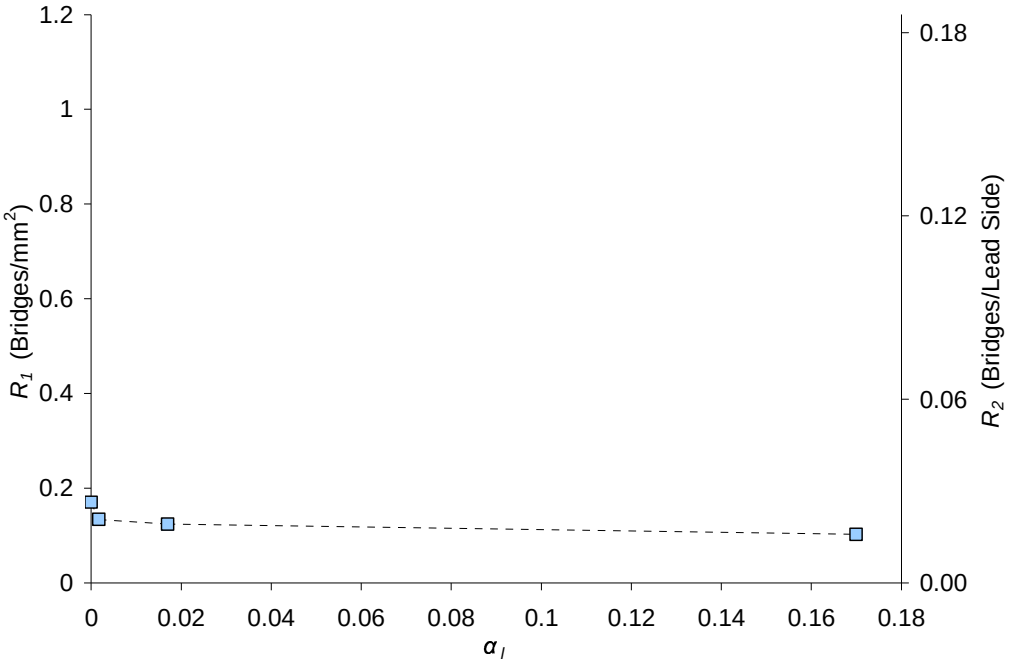

Fig. 16: Bridging Risk Metrics R_1 and R_2 versus the lower whisker fraction fractile, α_l.

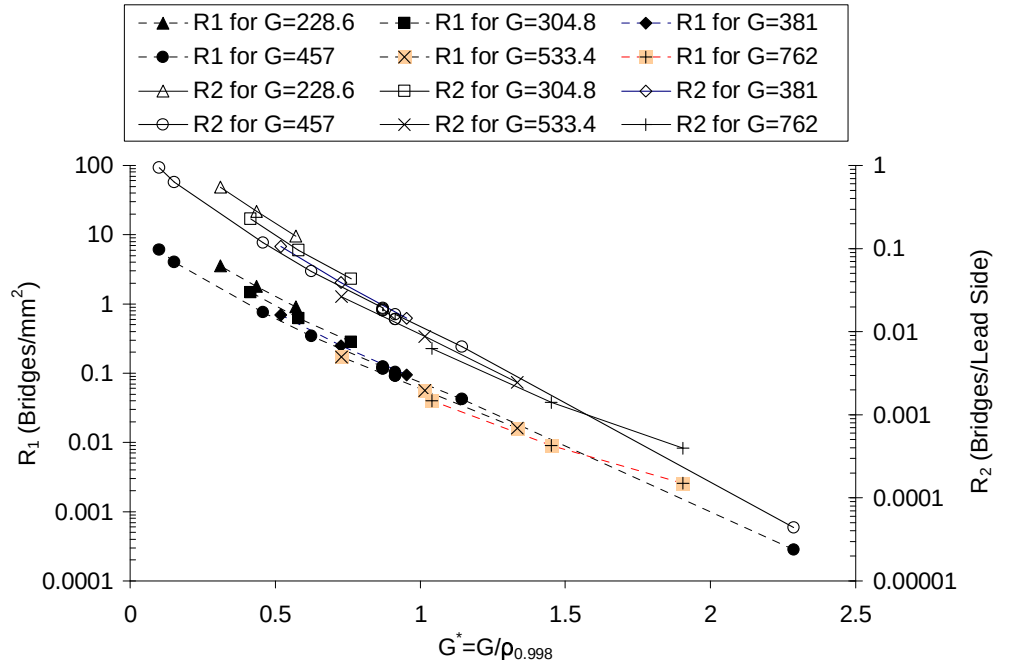

Fig. 17: Bridging risk metrics R_1 and R_2 versus dimensionless gap spacing G^* for various gap spacings and $\rho_{0.998}$ values.

Lead Thickness and Length

In this section, the whisker-bridging risk was evaluated for various lead thicknesses and lead lengths, as summarized in Table 6. During theses comparisons, gap spacing and whisker distributions were not varied. To improve the interpretation of results between plots, the data symbols with a (+) were used to designate the lead geometry data point for T = 152.4 microns, L = 1,016 microns and G = 457.2 microns in the subsequent figures. In the first portion of the lead geometry risk analysis, the bridging risk was plotted against dimensionless lead thickness, $T^* = T/G$, with G = 457 microns, and L = 1,016 microns. As is seen in Fig. 18, the bridging risk for the thinnest lead modeled (T = 25.4 microns) was 0.000881 bridges/lead side, which was two orders of magnitude less than the 0.0182 bridges/lead side risk associated with a typical 152.4-micron-thick lead. At the lower limit of lead thickness, the bridging risk approaches zero for two reasons. The first reason is that the area available to grow whiskers is reduced, limiting the number of whiskers that can be grown. The second reason for the decline in bridging risk is that as T becomes smaller, the shrinking target area restricts the number of possible growth-angle and base-position combinations that can yield a bridge. It should be noted that for very small lead thicknesses with small conductor separations, the parallel-plate modeling assumption may begin to break down and bridging-risk contributions from other surfaces may become important. On the other end of the spectrum of lead thickness, the bridging risk R_1 (bridges/mm^2) levels off to a constant value while the R_2 (bridges/lead side) continues to increase. This observation must be interpreted in the context of the R_1 and R_2 risk-metric definitions. Note that as lead thickness increases, at least three things contribute to increase the number of bridges. First, the number of whiskers capable of bridging increases as the lead source area increases. Second, the number of whisker-angle possibilities that can result in a bridge increases with increasing lead thickness. Finally, an increase in target area allows for more bridging. The R_1 parameter reaches a constant when T^* is greater than ~ *1* (Fig. 18). Although very thin leads are impractical from a handling and vibration or shock perspective, given a choice between a thicker lead and a thinner lead, it would be better from a Tin whisker risk standpoint to select the thinner lead. As will be discussed next, similar trends were observed as the lead length was varied.

In the evaluation of bridging risk while lead length was varied, the bridging risk was plotted against dimensionless lead length $L^* = L/G$, with G = 457 microns and T = 152 microns. The results shown in Fig. 19 are comparable to those observed in Fig. 18 and suggest that there is a lead length above which the additional bridging risk with increasing lead length is proportional to the lead area. In this case, the failures-per-unit area attained a relatively constant value between 0.1 and 0.12 when L^* was greater than ~1. As was observed in the lead thickness evaluation, the magnitude of R_2 (bridges/lead side) continued to increase with increasing lead length. As is seen in Fig. 19, the bridging risk for the 25.4-micron lead length was 0.000083 bridges/lead side, which is three orders of magnitude less than the 0.0182 bridges/lead side risk associated with a typical 1016-micron lead. From a practical perspective, a case where there is a very short lead length occurs when a hot-solder dip mitigation [29] inadvertently leaves Tin behind near the component body. The Monte Carlo modeling suggests that even imperfect hot-solder dipping can yield a significant reduction in Tin whisker-bridging risk.

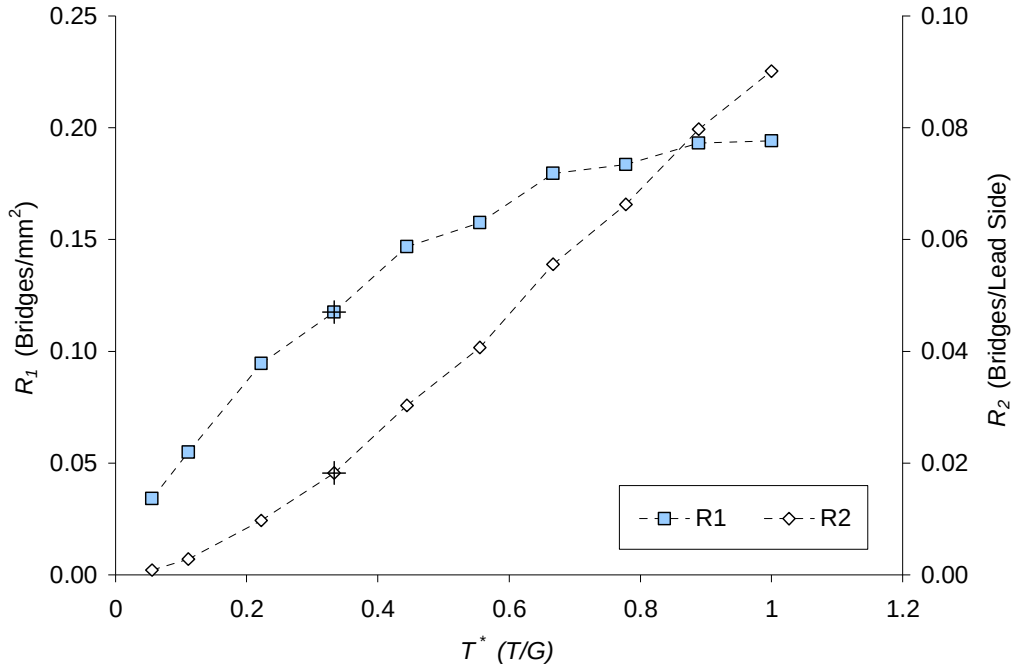

Fig. 18: Risk metrics R1 and R2 versus dimensionless lead thickness, T* = T/G with G = 457 microns

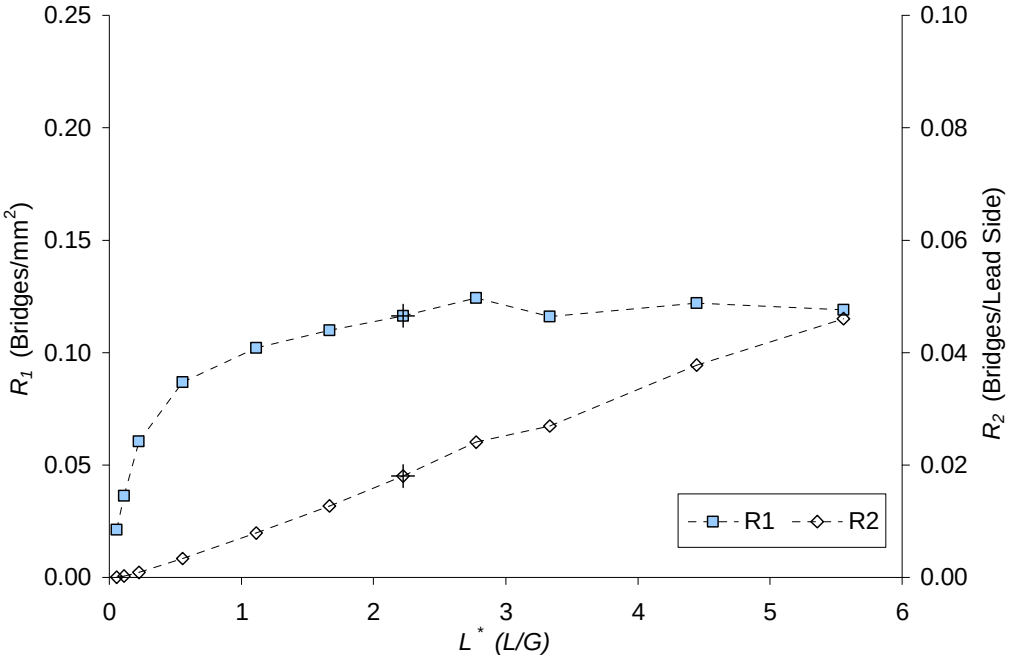

Fig. 19: Risk metrics R1 and R2 versus dimensionless lead length L* = L/G with G = 457 microns

Whisker-Bridging Risk Map

To facilitate an engineering evaluation at a system level, it is useful to understand the parameters that affect the bridging risk over the system's service life. In order to perform this assessment, a link must be established between upper fractile whisker length, $\rho_{0.998}$, and time. Regrettably, it is difficult, if not impossible, to determine what the expected whisker length will be on a component lead after it has been assembled in a certain way and exposed to a multitude of environmental (thermal, stress, and chemical) conditions through its life cycle. Nevertheless, a system-level bridging risk assessment capability is needed and is possible to construct. The Monte Carlo modeling approach described herein computes bridging risk for discrete values of $\rho_{0.998}$ taken to be representative of certain service times and environments. Performing the evaluation for various lead geometries allows a map of the bridging risk to be created.

Actual $\rho_{0.998}$ values can be obtained from a variety of sources such as long-term laboratory testing, extrapolation of short-term testing, and historical observations on fielded equipment, and are affected by the lead-base material; lead forming; plating process; mitigation efforts; the handling, storage, and service environments; and time. Alternatively, the $\rho_{0.998}$ parameter can be based on an understanding of the required mitigation level, environmental severity, and service life. For example, an analyst could find that seemingly different scenarios such as a severe environment combined with a short service-life requirement versus a benign environment with a long service life could result in similar bridging risks. Moreover, $\rho_{0.998}$ can be specified to gauge the increased risk associated with plating and other process mishaps. In the present work, the authors chose to use the test results from the long-term, room-temperature desiccated environment for bright-tin over copper-plated brass (specimen 11) obtained by Dunn [24] to create the bridging-risk map shown in Fig. 20 with the numeric summary given in Table 7. It should be noted that the effect on bridging risk due to the non-linear whisker growth characteristics are fully captured in the bridging-risk map.

While the bright-tin plating may not be representative of the low-stress platings currently used on electronic component leads (conservative), the dry-desiccated, room-temperature environment that these samples were exposed to was quite benign (non-conservative) compared to many high-performance applications used today. Two observations related to the Fig. 20 bridging-risk map are:

1. As the gap spacing was decreased below 457 microns, the bridging risk increased appreciably.
2. The smaller gap spacing exhibited a bridging risk that was more sensitive to the increase in upper-fractile whisker length, $\rho_{0.998}$.

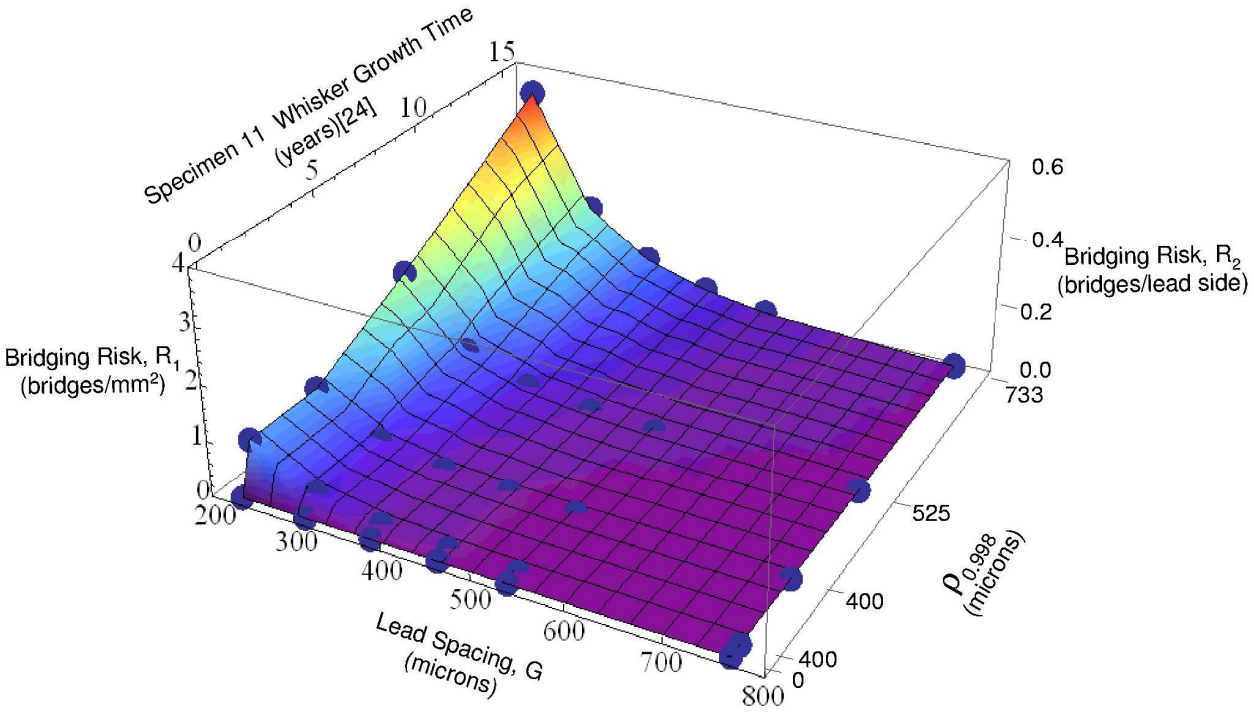

Fig. 20: Risk Map of metrics R1 and R2 lead-gap spacing and time for Dunn specimen 11. The plotting algorithm used interpolation among the data points to generate the three-dimensional plot.

SUMMARY

In the present study, several analytical ideas were arranged and sequenced, resulting in the formation of a unique, yet practical, modeling strategy capable of addressing the complex and probabilistic phenomena of Tin whisker bridging. These ideas fall primarily into two categories: whisker-length treatment and bridging-risk analysis.

Whisker length treatment

A dual-tail constraint strategy for producing probability-density functions for whisker lengths that incorporate measurements from different research experiments has been developed and applied herein. The strategy allows knowledge obtained from long-term whisker studies (for which a statistical understanding of the lengths have not been captured) to be merged with knowledge from shorter-term studies where a statistical understanding of the lengths is much stronger. By solving for the m and s lognormal parameters based on the dual constraints of ρ_{au}, and ρ_{al}, a set of PDFs can be constructed that provide a probabilistic insight into how whisker lengths progress over time. As more detailed measurements of whisker lengths become available, the ρ_{au}, and ρ_{al}, constraints can be appropriately refined, leading to a better understanding of the stochastic nature of whisker growth.

Bridging risk analysis

The dimensionless parameters $G^* = G/\rho_{0.998}$, $L^* = L/G$ and $T^* = T/G$ were used to capture bridging-risk trends and a whisker-bridging-risk map was generated for various lead-gap spacing values for a given whisker-growth-time evolution.

Manufactures and system integrators responsible for deploying high-reliability electronics will need to consider risk posed by Tin whiskers as the lead-free and RoHS (restriction of hazardous substances) legislation continues to increase the number of pure Tin components in the supply stream. It has been concluded herein that:

1. A versatile geometric and Monte Carlo-based model for bridging risk has been established that allows various mitigation levels, environmental conditions, and service times to be combined through the strategic selection of the $\rho_{0.998}$ parameter.
2. Reliability gains can be achieved by greatly reducing the bridging risk when Tin components having a dimensionless lead-to-lead gap spacing, G^*, greater than 1 are used, however additional Tin whisker mitigations may be necessary depending on the system requirements.
3. Tin-lead hot-solder dipping can significantly reduce whisker-bridging risk by reducing the length of the component lead available to form whiskers.

FUTURE WORK

In the future, the authors plan to perform further assessments of the $\rho_{0.998}$ and gap-spacing parameters in the three-dimensional risk map in order to create maps that show lines

of constant whisker-bridging risk. In addition, the authors think it would be beneficial to perform additional evaluations of the upper-fractile whisker length and fraction limits with other sets of experimental data. Furthermore, the authors would like to update the relationship between whisker length and time with additional whisker length observations from experimental and field data.

ACKNOWLEDGMENTS

The authors wish to thank Greg Hofmann for his support in verifying the lognormal distribution parameters needed to match the whisker fractiles and Paul Higgins for verifying the geometry solutions. In addition, they would like to thank Len Stefik and Clive Morris for their thoughtful review of the manuscript.

REFERENCES

[1] Hald A. Statistical Theory with Engineering Applications. John Wiley and Sons New York; 1965

[2] European Union (February 13, 2003). Directive 2002/95/EC/ of the European Parliament and of the Council of 27 January 2003 on the restriction of the use of certain hazardous substances in electrical and electronic equipment. Official Journal of the European Union

[3] Ganesan S, Pecht M. Lead-free electronics. John Wiley & Sons, Inc. USA; 2006.

[4] Brusse, J. Tin whisker observations on pure tin plated ceramic chip capacitors. AESF SUR/FIN Proceedings; June 24-27, 2002

[5] Brusse J, Leidecker H, Panashchenko L. Metal Whiskers: Failure Modes and Mitigation Strategies, Microelectronics Reliability & Qualification Workshop, hosted by The Aerospace Corporation, JPL and NASA, Manhattan Beach, CA; December 4-5, 2007 available at http://nepp.nasa.gov/whisker

[6] Osenbach JW, DeLucca JM, Potteiger BD, Amin A, Shook RL, and Baiocchi FA. Sn Corrosion and Its Influence on Whisker Growth, IEEE Transactions on Electronics Packaging Manufacturing 2007; 30(1):23-35

[7] Fukuda Y, Osterman M, and Pecht M. The Impact of Electrical Current, Mechanical Bending, and Thermal Annealing on Tin Whisker Growth, Microelectronics Reliability 2007; 47 9(1):88-92

[8] Mason M, Eng G. Understanding Tin Plasmas: A New Approach to Tin Whisker Risk Assessment, 2007 IEEE International Reliability Physics Symposium, Phoenix, AZ; April 15-19, 2007

[9] Fang T, Mathew S, Osterman M, Pecht W. Assessment of Risk Resulting from Unattached Tin Whisker Bridging, Circuit World 2007; 33(1):5-8

[10] GEIA-STD-0005-2. Standard for Mitigating the Effects of Tin Whiskers in Aerospace and High Performance Electronic Systems, Government Electronics and Information Technology Association; June 2006

[11] JP002. Current Tin Whiskers Theory and Mitigation Practices Guideline JEDEC/IPC Joint Publication; March 2006 [Online], Available at http://www.jedec.org/DOWNLOAD/search/JP002.pdf

[12] Galyon GT. Annotated tin whisker bibliography and anthology, IEEE Trans. in Elec. Packaging and Manufacturing 2005; 28(1):94-122.

[13] Amick P, Touw A, Condra L, Procarione W. Aerospace Response To Lead-Free Solder, On-Board Technology; April 2007 [pp. 34-37] http://www.onboard-technology.com/pdf_aprile2007/040706.pdf

[14] Fang T, Osterman M, Pecht M. A Tin Whisker Risk Assessment Algorithm, 38th International Symposium on Microelectronics, Reliability I (Issues in Packaging), Philadelphia, PA; September 25-29, 2005 [pp. 61-65]

[15] Hilty RD, Corman N. Tin Whisker Reliability Assessment by Monte Carlo Simulation, Proceedings of the IPC/JEDEC Lead-Free Symposium San Jose, CA; April 2005

[16] Touw AE and Lin TH. Tin Whisker Interactions: A Monte Carlo Analysis, CALCE Tin Whisker Symposium, Center for Advanced Life Cycle Engineering, University of Maryland, College Park, MD; April 24-25, 2007

[17] Mathew S, Osterman, M, Shibutani T, Yu Qiang. and Pecht M. Tin Whiskers: How to Mitigate and Manage the Risks, Proceedings of the IEEE International Symposium on High Density Packaging and Microsystem Integration, Shanghai, China; June 2007 [pp. 1 – 8]

[18] Pinsky D, Osterman M, Ganesan S. Tin Whiskering Risk Factors, IEEE Trans. Comp. Packaging Technol. 2004; 27(2):427-431

[19] Smetana J. Theory of Tin Whisker Growth: The End Game, IEEE Transactions on Electronics Packaging Manufacturing 2007; 30(1):11-22

[20] Boettinger WJ, Johnson CE, Bendersky LA, Moon K-W, Williams ME, Stafford GR. Whisker and Hillock formation on Sn, Sn-Cu and Sn-Pb electrodeposits, Acta Materialia 2005; 53:5033-5050

[21] Woodrow T. Tracer Diffusion in Whisker Prone Platings, Proceedings of the Surface Mount International Conference; September 2006

[22] Fang T, Osterman M, and Pecht M. Statistical Analysis of Tin Whisker Growth, Microelectronics Reliability, 2006; 46(5-6): 846-849

[23] Dunn B. A Laboratory Study of Tin Whisker Growth, ESA STR-223, European Space Research and Technology Centre Noordwijk, The Netherlands; September 1987.

[24] Dunn B. 15½ Years of Tin Whisker Growth – Results of SEM Inspections Made on Tin Electroplated C-Ring Specimens, ESTEC Materials Report 4562, European Space Research and Technology Centre Noordwijk, The Netherlands; March 22, 2006

[25] Wolfram Research, Inc., Mathematica, Version 6.0, Champaign, Illinois, 2007 http://www.wolfram.com/products/mathematica/index.html

[26] Panashchenko L, Mathew S, Osterman M, Pecht M. Tin Whisker Risk and Growth Assessment, CALCE Tin Whisker Symposium, Center for Advanced Life Cycle Engineering, University of Maryland, College Park, MD; April 24-25, 2007

[27] Fukuda Y, Osterman M, and Pecht M. Length Distribution Analysis for Tin Whisker Growth, IEEE Transactions on Electronics Packaging Manufacturing 2007; 30(1): 36-40

[28] Oberndorff P, Dittes M, Crema P, Su P, and Yu E. Humidity Effects on Sn Whisker Formation, IEEE Transactions on Electronics Packaging Manufacturing 2006; 29(4): 239-245

[29] GEIA-STD-0006. Requirements for Using Solder Dip to Replace the Finish on Electronic Piece Parts, Government Electronics and Information Association, Arlington, VA, USA; 2008

[30] Woodrow TA, Evaluation of Conformal Coatings as a Tin Whisker Mitigation Strategy, Part II. The Proceedings of SMTA International Conference, Rosemont, IL; September 24-28, 2006

[31] Kadesch JS, Leidecker H. Effects of Conformal Coat on Tin Whisker Growth, Proceedings of IMAPS Nordic, The 37th IMAPS Nordic Annual Conference; September 10-13, 2000 [pp. 108-116].

[32] McKeown SA, Kane J, Meschter SJ. Whisker Penetration into Conformal Coating, Conference Proceedings of IPC APEX 2007

[33] Meschter, S., and McKeown, S., "Effect of Hot Solder Dipping on Part Stresses," IMECE2008-66322, Proceedings of IMECE2008 ASME International Mechanical Engineering Congress and Exposition, Boston, Massachusetts, USA, October 31-November 6, 2008.